The Astrophysical Journal, 782:17 (12pp), 2014 February 10 doi:10.1088/0004-637X/782/1/17

THE CORE MASS GROWTH AND STELLAR LIFETIME OF THERMALLY PULSING ASYMPTOTIC GIANT BRANCH STARS

Jason S. Kalirai[1,2], Paola Marigo[3], and Pier-Emmanuel Tremblay[1,4,5]
[1] Space Telescope Science Institute, 3700 San Martin Drive, Baltimore, MD 21218, USA; jkalirai@stsci.edu
[2] Center for Astrophysical Sciences, Johns Hopkins University, Baltimore, MD 21218, USA
[3] Department of Physics and Astronomy, University of Padova, Vicolo dell'Osservatorio 3, I-35122 Padova, Italy; paola.marigo@unipd.it
[4] Zentrum für Astronomie der Universität Heidelberg, Landessternwarte, Königstuhl 12, D-69117 Heidelberg, Germany; ptremblay@lsw.uni-heidelberg.de
Received 2013 October 1; accepted 2013 December 16; published 2014 January 22

ABSTRACT

We establish new constraints on the intermediate-mass range of the initial–final mass relation, and apply the results to study the evolution of stars on the thermally pulsing asymptotic giant branch (TP-AGB). These constraints derive from newly discovered (bright) white dwarfs in the nearby Hyades and Praesepe star clusters, including a total of 18 high signal-to-noise ratio measurements with progenitor masses of $M_{\rm initial} = 2.8$–$3.8\,M_{\odot}$. We also include a new analysis of existing white dwarfs in the older NGC 6819 and NGC 7789 star clusters, $M_{\rm initial} = 1.6$ and $2.0\,M_{\odot}$. Over this range of initial masses, stellar evolutionary models for metallicity $Z_{\rm initial} = 0.02$ predict the maximum growth of the core of TP-AGB stars. By comparing the newly measured remnant masses to the robust prediction of the core mass at the first thermal pulse on the AGB (i.e., from stellar interior models), we establish several findings. First, we show that the stellar core mass on the AGB grows rapidly from 10% to 30% for stars with $M_{\rm initial} = 1.6$ to $2.0\,M_{\odot}$. At larger masses, the core-mass growth decreases steadily to ∼10% at $M_{\rm initial} = 3.4\,M_{\odot}$, after which there is a small hint of a upturn out to $M_{\rm initial} = 3.8\,M_{\odot}$. These observations are in excellent agreement with predictions from the latest TP-AGB evolutionary models in Marigo et al. We also compare to models with varying efficiencies of the third dredge-up and mass loss, and demonstrate that the process governing the growth of the core is largely the stellar wind, while the third dredge-up plays a secondary, but non-negligible role. Based on the new white dwarf measurements, we perform an exploratory calibration of the most popular mass-loss prescriptions in the literature, as well as of the third dredge-up efficiency as a function of the stellar mass. Finally, we estimate the lifetime and the integrated luminosity of stars on the TP-AGB to peak at $t \sim 3$ Myr and $E = 1.2 \times 10^{10}\,L_{\odot}$ yr for $M_{\rm initial} \sim 2\,M_{\odot}$ ($t \sim 2$ Myr for luminosities brighter than the red giant branch tip at $\log(L/L_{\odot}) > 3.4$), decreasing to $t = 0.4$ Myr and $E = 6.1 \times 10^{9}\,L_{\odot}$ yr for stars with $M_{\rm initial} \sim 3.5\,M_{\odot}$. The implications of these results are discussed, especially with respect to general studies aimed at characterizing the integrated light output of TP-AGB stars in population synthesis models.

Key words: open clusters and associations: individual (Hyades and Praesepe) – stars: AGB and post-AGB – stars: evolution – techniques: photometric – techniques: spectroscopic – white dwarfs

Online-only material: color figures

1. INTRODUCTION

The life cycles of most stars are dominated by quiescent, long-lived phases such as the hydrogen-burning main sequence and the white dwarf cooling sequence. For low- and intermediate-mass stars with initial masses in the range $1\,M_{\odot} \gtrsim M_{\rm initial} \gtrsim 6$–$8\,M_{\odot}$, these two extremes are connected by the thermally pulsing asymptotic giant branch (TP-AGB) evolutionary phase, during which stars experience quasi periodic thermal instabilities of the He-burning shell (thermal pulses) and rapidly lose a large fraction of their mass (Herwig 2005).

An understanding of the TP-AGB phase has many important applications in astronomy. Of particular interest is the prospect of directly measuring the growth of the stellar core on the AGB. The growth is set by the lifetime of the TP-AGB, which itself depends on the timescale over which the stellar envelope is lost through mass loss processes (Marigo & Girardi 2001). At the same time, the effective increase of the core may be limited by the third dredge-up, which causes a sudden reduction of its mass each time it takes place (Herwig 2004). This growth of the core mass and the TP-AGB lifetime as a function of the initial stellar mass (hence age) are powerful inputs to theoretical models aimed at evaluating the integrated luminosity contribution of AGB stars, since these luminosities play a central role in the construction of population synthesis models that are used to interpret galaxy evolution (e.g., Bruzual & Charlot 2003; Maraston et al. 2006; Conroy et al. 2009: Conroy & Gunn 2010; Zibetti et al. 2013).

On the other hand it is a matter of fact that, in spite of the remarkable progress attained in fields of TP-AGB stellar evolution in the last decades (see Herwig 2005, for a review), predictions of this phase are still affected by a sizable degree of uncertainty. This should be mostly ascribed to the high complexity of the physics involved, and the fact we still have to cope with ill-defined theories of stellar mixing and convection, as well as insufficient understanding of mass loss mechanisms. We still lack an accurate knowledge of how the third dredge-up episodes vary with thermal pulses, and of what is the dependence of their efficiency on stellar mass and metallicity. Likewise, substantial effort is needed to gain insight into the driving mechanism and strengths of stellar winds on the AGB (e.g., Habing 1996; Weidemann 2000; Willson 2000; Gustafsson &

[5] Hubble Fellow.

Höfner 2004). The relation between mass loss and other stellar parameters such as metallicity and dust-to-gas ratio is also not well understood. Similarly, direct observational constraints are difficult to establish given the dust enshrouded nature of AGB stars and their short evolutionary lifetimes.

The relation between the initial and final (i.e., white dwarf) masses of stars represents a new tool to bear on studies of AGB evolution (Bird & Pinsonneault 2011), since the end product of AGB stars is the white dwarf cooling sequence (e.g., Weidemann 2000; Girardi et al. 2010). The relation has now been well-measured by spectroscopically studying white dwarfs that are members of star clusters with well defined characteristics. The current constraints from $M = \sim$1–7 $M_{\odot}$ shows a rise in the remnant mass that is proportional to the initial mass (e.g., see Kalirai et al. 2007; 2008; 2009 and references therein). At the intermediate masses that are characteristic of AGB stars, the relation exhibits a large scatter and this leads to difficulty in ascertaining the influence of AGB evolution. This scatter is likely caused by the heterogeneous nature of previous studies. The white dwarf spectra have been collected with different instrumentation and suffer from many selection effects and biases. For example, there is likely contamination in the sample from field stars, low signal-to-noise ratio measurements, fits to Balmer lines using outdated spectroscopic models, incorrect metallicity assumptions, and inaccurate turnoff ages inferred from different theoretical isochrones (leading to systematic errors in the initial masses).

Bird & Pinsonneault (2011) recently investigated the initial–final mass relation and employed a fuel consumption argument to set a lower bound on the fraction of light emitted during the TP-AGB phase. Their results, based on combining several studies of the initial–final mass relation, suggest that the growth of the stellar core exhibits a plateau of ∼20% at $M_{\rm initial} \sim 3\,M_{\odot}$, decreasing to ∼10% at $M_{\rm initial} > 4\,M_{\odot}$. In the present study, we build on the initial work by Bird & Pinsonneault (2011) by taking advantage of new observational and theoretical work. First, we minimize systematic errors by limiting our study to a small set of star clusters that all have moderately super-Solar metallicity, two of which also have identical ages.[6] Second, we take advantage of newly discovered white dwarfs in both the Hyades and Praesepe star clusters to increase the significance of the measurement over the critical mass range that corresponds to expected AGB evolution. Finally, we largely eliminate systematic errors in the derivation of remnant masses by re-calculating all measurements with a common set of white dwarf spectral models that incorporate the latest physics of the Stark broadening. The result of this work is a robust measurement of the core-mass growth at $M_{\rm initial} = 1.6$ to 3.8 $M_{\odot}$.

We describe the observational data set in Section 2 and the calculation of initial and final masses for each star in Section 3. These results provide new constraints on the absolute core-mass growth of the AGB (Section 4), the processes governing core-mass growth including the significance of the third dredge up (Section 5.1) and mass loss (Section 5.2), and the lifetime and energy output of these stars (Section 6). All of the results are discussed with respect to the important role that the TP-AGB phase of stellar evolution plays in establishing the fraction of red light emitted in population synthesis models.

[6] The nine star clusters in Bird & Pinsonneault (2011) spanned a metallicity range of greater than a factor of two.

2. NEW WHITE DWARFS IN THE HYADES AND PRAESEPE STAR CLUSTERS

The Hyades and Praesepe open star clusters share incredible similarities. Both clusters have ages of ∼600–650 Myr and metallicities slightly higher than Solar, $Z_{\rm initial} \sim 0.02$ (Gratton 2000; An et al. 2008), and can be studied in exquisite detail given their proximity ($d = 46.3$ pc for Hyades—Perryman et al. 1998; $d = 184.5$ pc for Praesepe—An et al. 2008). The present main-sequence turnoff mass in these clusters is $\sim$3 $M_{\odot}$.

Recent observations of both the Hyades and Praesepe clusters have revealed new members of the remnant white dwarf population. For the Hyades, Schilbach & Röser (2012) constructed a multi-step process to identify 27 white dwarf *candidates*, including all 10 of the previously known members (van Altena 1969; Reid 1992; Weidemann et al. 1992; von Hippel 1998). Their methods combine tangential motions from proper motion measurements, photometric comparisons with the white dwarf locus in the color–magnitude diagram, and radial velocities for some stars. Tremblay et al. (2012) further scrutinized the membership of these candidates by fitting state-of-the art spectral models to the Balmer lines (Tremblay & Bergeron 2009), and calculating both atmospheric parameters (e.g., $\log(g)$, $T_{\rm eff}$, and cooling age) and theoretical luminosities. Tremblay et al. (2012) also simulated the field contamination along this sightline in their analysis. By comparing the spectroscopic and kinematic distances, as well as the cooling ages of the new stars to the cluster age, they confirmed five of the new candidates as likely members of the Hyades.[7] The other candidates are not explicitly excluded from membership. Radial velocities of several of these candidates were also observed by Zuckerman et al. (2013), who confirm three of the new candidates as bona-fide members of the Hyades, but also reject WD0743+442. The final list of Hyades members that we consider, including these new stars and the seven classical members that are not in binaries, is presented in Table 1. The atmospheric parameters for these stars have been taken directly from Tremblay et al. (2012).

For the Praesepe, earlier studies measured five white dwarf candidates (Luyten 1962; Eggen & Greenstein 1965; Anthony-Twarog 1982, 1984; Claver et al. 2001), and more recent observations have identified an additional six white dwarf candidates (Dobbie et al. 2004, 2006). Casewell et al. (2009) present a careful examination of nine of these stars, based on high-resolution optical spectroscopy, and show contamination in the sample from a magnetic white dwarf and a likely field white dwarf. Their final sample of Praesepe white dwarf members includes seven white dwarfs, which are listed in Table 1 (although, see below for the atmospheric properties of these stars).

3. INITIAL AND FINAL MASSES

The atmospheric properties of the 4 white dwarfs in NGC 6819 and NGC 7789, and the 18 white dwarfs in the Hyades and Praesepe clusters are listed in Table 1. These properties, including the white dwarf masses ($M_{\rm final}$), were calculated by Kalirai et al. (2009), Tremblay et al. (2012) and Casewell et al. (2009) using the successful technique of fitting the Balmer lines in the spectra with model atmospheres (Bergeron et al. 1992). As has been demonstrated numerous times, this technique leads to accurate parameters provided the spectra have high signal-to-noise ratio and sensitivity to the higher order Balmer lines

[7] Hyades white dwarf WD0231-054 is excluded since the photometric temperature doesn't agree with the spectroscopic temperature.

Table 1
Hyades and Praesepe Cluster White Dwarfs

Cluster	ID	$T_{\rm eff}$ (K)	log g	$M_{\rm final}$ ($M_\odot$)	log($t_{\rm cool}$) (yr)	$M_{\rm initial}$ ($M_\odot$)
NGC 6819	NGC 6819_6	21,900 ± 300	7.89 ± 0.04	0.56 ± 0.02	7.56 ± 0.04	$1.60^{+0.06}_{-0.05}$
NGC 6819	NGC 6819_7	16,600 ± 200	7.97 ± 0.04	0.59 ± 0.02	8.14 ± 0.04	$1.62^{+0.07}_{-0.05}$
NGC 7789	NGC 7789_5	31,600 ± 200	7.98 ± 0.05	0.64 ± 0.03	6.95 ± 0.05	$2.02^{+0.07}_{-0.14}$
NGC 7789	NGC 7789_8	25,000 ± 400	8.06 ± 0.07	0.66 ± 0.04	7.46 ± 0.07	$2.02^{+0.09}_{-0.11}$
Hyades	WD0352+096	14,670 ± 380	8.30 ± 0.05	0.80 ± 0.03	8.53 ± 0.05	$3.59^{+0.21}_{-0.15}$
Hyades	WD0406+169	15,810 ± 290	8.38 ± 0.05	0.85 ± 0.03	8.50 ± 0.04	$3.49^{+0.13}_{-0.10}$
Hyades	WD0421+162	20,010 ± 320	8.13 ± 0.05	0.70 ± 0.03	7.97 ± 0.06	$2.90^{+0.02}_{-0.02}$
Hyades	WD0425+168	25,130 ± 380	8.12 ± 0.05	0.71 ± 0.03	7.49 ± 0.08	$2.79^{+0.01}_{-0.01}$
Hyades	WD0431+126	21,890 ± 350	8.11 ± 0.05	0.69 ± 0.03	7.78 ± 0.07	$2.84^{+0.02}_{-0.02}$
Hyades	WD0437+138	15,120 ± 360	8.25 ± 0.09	0.74 ± 0.06	8.47 ± 0.07	$3.41^{+0.21}_{-0.15}$
Hyades	WD0438+108	27,540 ± 400	8.15 ± 0.05	0.73 ± 0.03	7.30 ± 0.09	$2.78^{+0.01}_{-0.01}$
Hyades	WD0348+339	14,820 ± 350	8.31 ± 0.05	0.80 ± 0.03	8.52 ± 0.05	$3.55^{+0.19}_{-0.14}$
Hyades	HS0400+1451	14,620 ± 60	8.25 ± 0.01	0.76 ± 0.01	8.50 ± 0.01	$3.49^{+0.03}_{-0.03}$
Hyades	WD0625+415	17,610 ± 280	8.07 ± 0.05	0.66 ± 0.03	8.12 ± 0.05	$2.97^{+0.03}_{-0.03}$
Hyades	WD0637+477	14,650 ± 590	8.30 ± 0.06	0.80 ± 0.04	8.53 ± 0.06	$3.59^{+0.26}_{-0.18}$
Praesepe	WD0833+194	15,252 ± 41	8.28 ± 0.01	0.79 ± 0.04	8.47 ± 0.05	$3.41^{+0.16}_{-0.09}$
Praesepe	WD0836+199	14,971 ± 60	8.33 ± 0.01	0.82 ± 0.04	8.53 ± 0.05	$3.59^{+0.18}_{-0.13}$
Praesepe	WD0837+185	15,476 ± 60	8.41 ± 0.01	0.87 ± 0.04	8.55 ± 0.05	$3.66^{+0.21}_{-0.16}$
Praesepe	WD0837+199	17,640 ± 38	8.30 ± 0.01	0.80 ± 0.04	8.30 ± 0.05	$3.13^{+0.06}_{-0.05}$
Praesepe	WD0840+190	15,335 ± 68	8.48 ± 0.01	0.91 ± 0.05	8.61 ± 0.05	$3.97^{+0.40}_{-0.24}$
Praesepe	WD0840+200	15,383 ± 42	8.28 ± 0.01	0.79 ± 0.04	8.46 ± 0.05	$3.39^{+0.12}_{-0.09}$
Praesepe	WD0843+184	15,418 ± 50	8.44 ± 0.01	0.89 ± 0.05	8.57 ± 0.05	$3.77^{+0.27}_{-0.18}$

(Kleinman et al. 2013). However, both the Kalirai et al. (2009) and Casewell et al. (2009) studies modeled the white dwarf spectra using older line profiles compared to those presented in Tremblay & Bergeron (2009). We therefore apply a small correction to these results to place them on the same foundation as the new Hyades measurements (i.e., from Figure 12 in Tremblay & Bergeron 2009). For example, for the Praesepe white dwarfs, this correction is +400 K in $T_{\rm eff}$ and +0.1 dex in log(g). All of the updated atmospheric properties, including the final masses of the white dwarfs, are presented in Table 1.

Progenitor masses for these white dwarfs can be calculated by taking advantage of their membership in the four clusters (e.g., see Kalirai et al. 2005 for a similar study in another intermediate age cluster). First, the mass and temperature of each white dwarf uniquely sets its cooling age ($t_{\rm cool}$), which represents the time since that white dwarf left the tip of the AGB. By subtracting this cooling age from the age of the star cluster, we arrive at the lifetime of the progenitor star that made the white dwarf (i.e., the dominant main-sequence lifetime plus the post main-sequence lifetime up to the tip of the AGB). The ages of the clusters are taken from earlier studies—2.5 Gyr for NGC 6819 and 1.4 Gyr for NGC 7789 (Kalirai et al. 2001, 2008), and 625 Myr for the Hyades and Praesepe (Perryman et al. 1998; Claver et al. 2001). The progenitor masses of the stars ($M_{\rm initial}$) follow from standard stellar models at the cluster metallicity, and are listed in the last column of Table 1 (new Bressan et al. 2012 models). The sensitivity of these initial masses to mild changes in the metallicity or age of the star clusters is small. For example, a shift in the age from the default 625 Myr by ±50 Myr leads to initial masses that are <3% smaller or larger, and a change in the metallicity of $\Delta Z = 0.05$ leads to a similar effect on the masses. Such effects on the ages of the older clusters NGC 6819 and NGC 7789 lead to even smaller uncertainties.

Table 2
Summary of Initial–Final Mass Pairs for Each Cluster

Cluster	$M_{\rm initial}$ ($M_\odot$)	$M_{\rm final}$ ($M_\odot$)	Integrated Mass Loss Through Post-Main Sequence Evolution (%)
NGC 6819	1.61 ± 0.01	0.575 ± 0.015	64.3
NGC 7789	2.02 ± 0.00	0.650 ± 0.010	67.8
Hyades	3.22 ± 0.11	0.749 ± 0.017	76.8
Praesepe	3.56 ± 0.10	0.837 ± 0.020	76.5

The individual measurements for stars in each cluster presented in Table 1 are averaged into four initial–final mass pairs in Table 2. Also included is the resulting integrated mass loss through stellar evolution. For $M_{\rm initial} \sim 3\ M_\odot$, our results demonstrate that stars will lose 75% of their mass to the interstellar medium (ISM). As expected, the mass loss is measured to be very similar for the Hyades and Praesepe clusters, given their identical age and metallicity.

4. CORE-MASS GROWTH ON THE TP-AGB

The core mass at the first thermal pulse, $M_{\rm c,1tp}$, is primarily a function of initial stellar mass and chemical composition. A general agreement exists among different stellar evolution models on the trend of $M_{\rm c,1tp}$ with the stellar mass. For instance, a minimum of $M_{\rm c,1tp}$ is expected in correspondence to the maximum mass, $M_{\rm He-F}$, for a star to develop an electron degenerate He-core, while the first occurrence of the second dredge-up in intermediate-mass ($M_{\rm initial} \simeq$ 3–4 $M_\odot$) produces a change in the slope (inflection point) of the $M_{\rm c,1tp}$–$M_{\rm initial}$ relation that runs flatter at higher masses. Clearly, precise predictions of these features do depend on the physics adopted

in stellar models (see, e.g., Wagenhuber & Groenewegen 1998). However, the current theoretical dispersion in $M_{\rm c,1tp}$ is much smaller than the uncertainties in the final masses due to the uncertainties in the subsequent TP-AGB evolution. In this sense, $M_{\rm c,1tp}$ may be considered a robust prediction of stellar models.

We take $M_{\rm c,1tp}$ from the new stellar evolutionary models in Bressan et al. (2012) (i.e., the PARSEC code: PAdova & TRieste Stellar Evolution Code) for initial composition $Z_{\rm initial} = 0.02$, $Y_{\rm i} = 0.284$, with a scaled-solar distribution of metal abundances according to Caffau et al. (2011),—this corresponds to Solar metallicity $Z_{\odot} = 0.01524$. For example, over the range of initial masses spanned by the Hyades and Praesepe white dwarfs in Table 1, $M_{\rm c,1tp} = 0.60\,M_{\odot}$ at $M_{\rm initial} = 2.8\,M_{\odot}$, $M_{\rm c,1tp} = 0.70\,M_{\odot}$ at $M_{\rm initial} = 3.3\,M_{\odot}$, and $M_{\rm c,1tp} = 0.76\,M_{\odot}$ at $M_{\rm initial} = 3.8\,M_{\odot}$.

Beyond the first thermal pulse, the subsequent TP-AGB is challenging to model because of the complex interplay of many physical processes, which are often affected by severe uncertainties. During this phase, the mass of the H-exhausted core increases following the outward advancement of the H-burning shell during the quiescent inter-pulse periods, while the mass may be temporarily reduced at each third dredge-up event, by an amount that depends on the depth of the envelope penetration. In the meantime the stellar envelope is progressively lost by stellar winds. Therefore, the size of stellar core increase is controlled by the competition between (1) the speed of displacement of the H-burning shell, that fixes the core growth rate, (2) the strength of mass loss, that determines the TP-AGB timescale, and (3) the efficiency of the third dredge-up (if it occurs), that lessens the effective mass increment. While the former aspect mainly relies on well-established properties of nuclear reactions, the latter two processes, i.e., mass loss and third dredge-up, are still not robustly assessed on theoretical grounds. For more information, see Marigo & Girardi (2001); Marigo (2013).

The end product of the TP-AGB is the nuclear-processed core, the C-O white dwarf. The masses of the 22 white dwarfs in Table 1 therefore provide a novel method to directly measure the core growth on the TP-AGB, $\Delta M_{\rm growth} = M_{\rm final} - M_{\rm c,1tp}$. We illustrate this in Figure 1, both for the individual raw data (open circles with error bars) and five (straight) average values across the initial mass spectrum. The averages are calculated by treating each of the NGC 6819 and NGC 7819 pairs separately, and then defining three mass bins between $2.5 < M < 4.0\,M_{\odot}$ with bin width $0.5\,M_{\odot}$ for the 18 Hyades and Praesepe white dwarfs. The averages are shown as darker filled circles and connected with a thick black line. The uncertainties in these values are the errors in the mean for each average. The core-mass growth is shown as a percentage, $\Delta M_{\rm growth}/M_{\rm c,1tp}$. The binned averages illustrates that $\Delta M_{\rm growth}$ increases rapidly from 10% to 30% for stars with $M_{\rm initial} = 1.6$ to $2.0\,M_{\odot}$, and at larger masses decreases down to $\sim$10% at $M_{\rm initial} = 3.4\,M_{\odot}$. There is a small hint of an upturn at larger masses, suggesting that the core-mass growth is $\gtrsim$10% up to $M_{\rm initial} = 3.8\,M_{\odot}$.

For $M_{\rm initial} > 3\,M_{\odot}$, our results are systematically lower than those reported in the similar study by Bird & Pinsonneault (2011), by as much as a factor of two. Although their study also looked at white dwarfs in the Hyades and Praesepe clusters (not including the new discoveries and uniform measurements from the Tremblay et al. 2012 models), they also included white dwarf measurements in two other star clusters over this mass range (i.e., with different ages and metallicities).

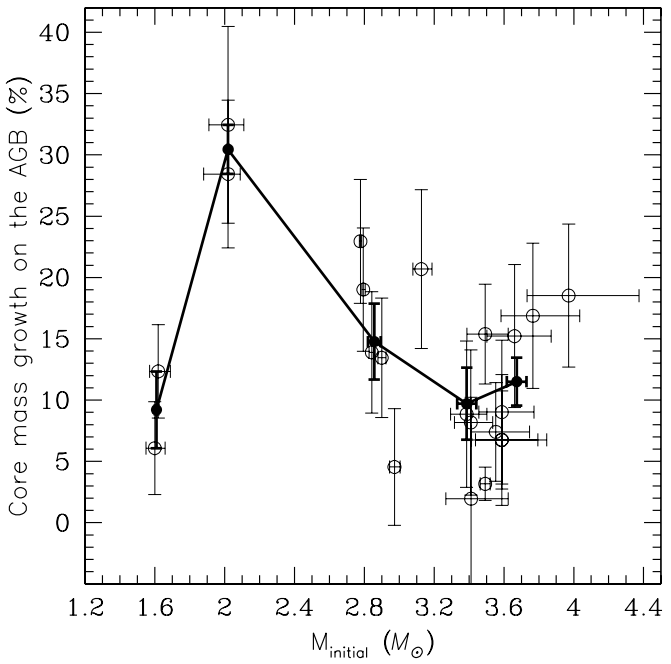

Figure 1. Growth of the stellar core on the TP-AGB ($\Delta M_{\rm growth} = M_{\rm final} - M_{\rm c,1tp}$), measured by comparing the masses of bright white dwarfs in four star clusters ($M_{\rm final}$; see Section 3) to the core mass at the first thermal pulse from the new Bressan et al. (2012) stellar models ($M_{\rm c,1tp}$; see Section 4). The data points with error bars illustrate individual measurements in the four star clusters, and the solid black line shows average values (and errors in the averages) across five $M_{\rm initial}$ bins as described in Section 4. The maximum growth of the stellar core of AGB stars occurs for stars with $M_{\rm initial} \sim 2.0\,M_{\odot}$.

5. TESTING TP-AGB MODELS

The measurement of $\Delta M_{\rm growth}$ over $M_{\rm initial} = 1.6$–$3.8\,M_{\odot}$ provides a new test to the latest evolutionary models of TP-AGB stars. New calculations by Marigo et al. (2013) offer significant advances over previous generation models. These models begin at the first thermal pulse, extracted from the new Bressan et al. (2012) stellar models, and continue to the complete ejection of the envelope due to winds (Marigo et al. 2008). Compared to past releases (Marigo & Girardi 2007; Girardi et al. 2010) the new tracks now include a more accurate treatment of the star's energetics (the core mass–luminosity relation and its breakdown due to hot-bottom burning are self-consistently predicted), and rely on the first ever on-the-fly computations of detailed molecular chemistry and gas opacities (Marigo & Aringer 2009). This new advance guarantees full consistency between the envelope structure and the surface chemical abundances, and therefore robustly tracks the impact of third dredge-up episodes and hot-bottom burning.

In this work, we explore the dependence of the predicted final mass left at the end of the TP-AGB phase to 1.) the efficiency of the third dredge-up, and 2.) the mass loss, starting from a reference set of TP-AGB models, as described in Marigo et al. (2013). The occurrence of the third dredge-up is determined with the aid of envelope integrations at the stage of the post-flash luminosity peak, checking if the condition $T_{\rm bce} > T_{\rm dred}$ is fulfilled, i.e., the temperature at the base of the convective envelope exceeds a minimum value (more details in Marigo et al. 2013). For the present calculations we set $\log(T_{\rm dred}) = 6.6$, a value somewhat larger than the $\log(T_{\rm dred}) = 6.4$ that was assumed for the test models presented in Marigo et al. (2013). Increasing $T_{\rm dred}$ causes a later onset of the third dredge-up,

i.e., at larger core masses, which is a more suitable choice for describing the formation of carbon stars at higher metallicities, as suggested by previous full model calculations (Karakas et al. 2002) and calibration studies (Marigo et al. 1999).

The efficiency[8] of the third dredge-up λ, as a function of stellar mass and metallicity, is taken from the relations of Karakas et al. (2002, hereafter also K02), that fit the results of their full TP-AGB models. The K02 formalism represents our initial prescription for the third dredge-up, which will be then varied to explore the sensitivity of the predicted final masses to different efficiencies of the mixing episodes, and to eventually obtain calibrated relations for λ as a function of the stellar mass. The mass loss prescription is similar to that adopted in Girardi et al. (2010). The Reimers mass loss formulation with an efficiency parameter $\eta = 0.2$ (following the recent asteroseismologic calibration of Miglio et al. 2012) is assumed in the initial stages, followed by an exponentially increasing mass-loss rate relation, derived from computations of periodically-shocked dusty atmospheres (Bedijn 1988).

Similar to other descriptions, the Marigo et al. (2013) models take the efficiencies of both the third dredge-up and mass loss as free parameters, to be calibrated with observations. Indeed, the initial–final mass relation provides us with an important tool to put constraints on these two processes. In this perspective, besides the default choice of parameters, we consider several additional prescriptions for both processes. Given its flexibility, physical accuracy, and fast performance, the COLIBRI code developed by Marigo et al. (2013) is an appropriate tool to carry out extensive exploration and calibration analyses.

5.1. Characterizing the Significance of the Third Dredge-Up

The third dredge-up affects the core-mass growth on the TP-AGB in two main modes.

The first effect is the *direct* reduction of its mass: every time a dredge-up episode takes place with an efficiency λ, the core mass is almost instantaneously turned down by an amount $\lambda \Delta M_c$. Unfortunately, the efficiency λ is one of the most uncertain parameters of TP-AGB star modeling as it is found to vary significantly from study to study, depending on the adopted treatment of convection, mixing, and numerics (see, e.g., Marigo 2012 for a review).

An *indirect* effect is driven by the changes in the surface chemical composition caused by the penetration of the base of the convective envelope into the inter-shell region. In fact, each dredge-up event results in a mixing of material (mainly ^{4}He, ^{12}C, ^{22}Ne, Na, Mg and Al isotopes, and slow-neutron capture elements) left by the pulse-driven convective zone to the outer layers. In particular, the enrichment in primary carbon causes the surface C/O ratio to increase. As soon as the number of carbon atoms exceeds that of oxygen (i.e., C/O > 1) an abrupt change in the molecular equilibria causes a sudden rise of the atmospheric opacity (Marigo 2002). In turn, this results in lower effective temperatures and increased mass loss from dust-driven winds (Marigo & Girardi 2007; Mattsson et al. 2010). As a consequence, the TP-AGB lifetime is shorter and the growth of the core mass is smaller than otherwise predicted neglecting the enhancement of the carbon-bearing opacity.

According to the K02 models, λ quickly increases from one thermal pulse to another until it reaches a maximum, $\lambda_{\rm max}$, whose value typically increases with the stellar mass, while it decreases at larger metallicity. To explore the effect of the third dredge-up, we vary its efficiency by simply multiplying the original K02 $\lambda_{\rm max}$ by four selected factors, i.e., $\lambda_{\rm max} = \xi_\lambda \lambda_{\rm max}^{\rm K02}$, with $\xi_\lambda = 0.0, 0.5, 0.8, 1.0$, as shown in Figure 2. They represent a sequence of increasing efficiency of the third dredge-up, starting from no dredge-up ($\xi_\lambda = 0.0$), up to recover the reference K02 relations ($\xi_\lambda = 1.0$). Since this latter case yields already rather large efficiencies ($\lambda_{\rm max} \gtrsim 0.8$–$0.9$) for intermediate-mass stars ($M_{\rm initial} > 2.5\,M_\odot$), we do not consider larger value, i.e., $\xi_\lambda > 1.0$.

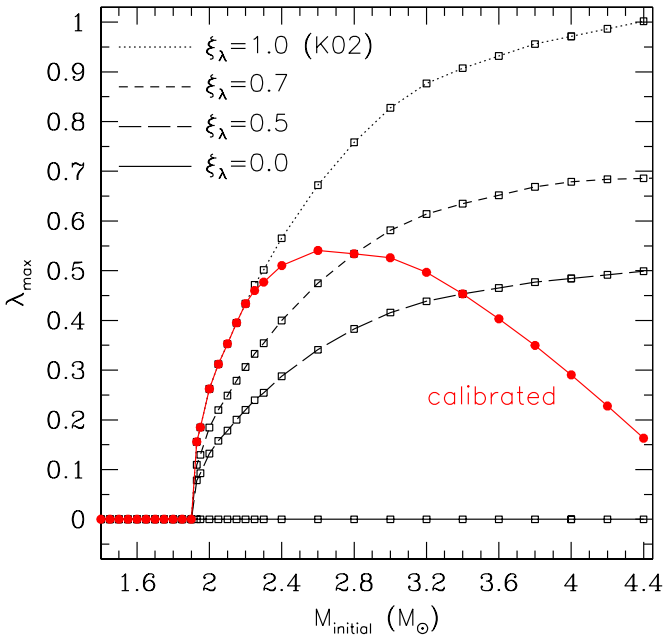

Figure 2. Maximum efficiency, $\lambda_{\rm max}$, of the third dredge-up attained during the TP-AGB evolution as a function of the initial stellar mass. The four curves correspond to selected values of the variation factor ξ_λ, defined by the relation $\lambda_{\rm max} = \xi_\lambda\, \lambda_{\rm max}^{\rm K02}$, where $\lambda_{\rm max}^{\rm K02}$ denotes the reference predictions of Karakas et al. (2002, K02). Note that $\xi_\lambda = 0$ refers to models without third dredge-up. The calibrated relation (red line connecting filled circles), based on the new observed average core-mass growth from our data, exhibits a non-monotonic behavior with the stellar mass.

(A color version of this figure is available in the online journal.)

Based on the four curves in Figure 2, we calculate theoretical sequences for TP-AGB evolution, and illustrate the resulting core mass growth in Figure 3. All of the predictions have the same shape and approximate normalization as the new observations (darker line with filled circles). This agreement is a remarkable validation of these models at $Z_{\rm initial} = 0.02$, which lack strong observational tests. The top solid black curve predicts that the maximum core-mass growth in the absence of any third dredge-up reaches $\Delta M_{\rm growth} = 30\%$ at $M_{\rm initial} \sim 2\,M_\odot$, decreasing steadily to $\Delta M_{\rm growth} = 23\%$ at $M_{\rm initial} = 2.8\,M_\odot$ and $\Delta M_{\rm growth} = 11\%$ at $M_{\rm initial} = 3.8\,M_\odot$.

We note that for $M_{\rm initial} \lesssim 1.9\,M_\odot$ all the curves coincide, since at these masses and for $Z_{\rm initial} = 0.02$ the third dredge-up is expected not to take place. At larger masses, $M_{\rm initial} \gtrsim 1.9\,M_\odot$, the curves start to deviate as a consequence of the third dredge-up. The three sequences below the top-most model ($\xi_\lambda = 0$) each correspond to the same mass-loss law (Bedijn 1988; see Section 5.2), but with increasing efficiency of the third dredge-up process (as indicated in the label). These models progressively predict a smaller growth in the stellar core, as expected given the direct reduction of the H-exhausted core

[8] The efficiency of the third dredge-up is usually expressed with $\lambda = (\Delta M_{\rm dup}/\Delta M_{\rm c})$, defined as the fraction of the core mass increment over an inter-pulse period ($\Delta M_{\rm c}$), that is dredged-up to the surface at the next thermal pulse (with mass $\Delta M_{\rm dup}$)

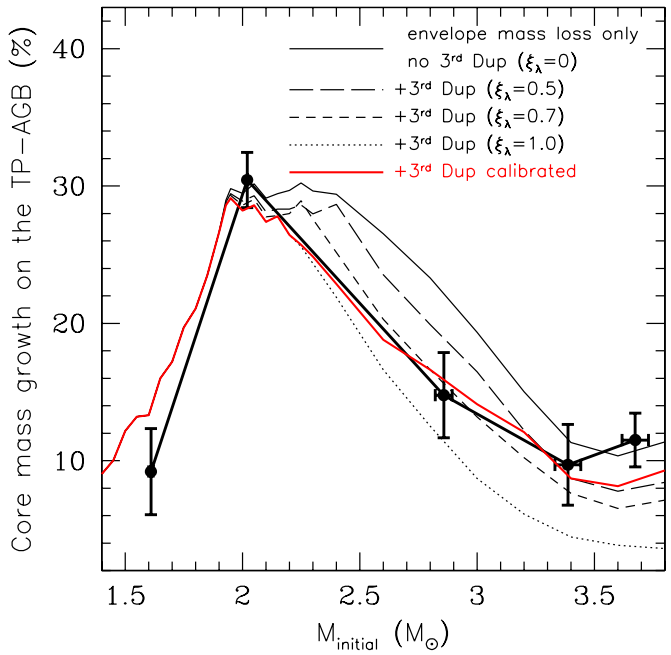

Figure 3. Our measurements for the growth of the stellar core on the TP-AGB is shown as a darker line with filled circles, and compared to five theoretical models of the TP-AGB phase of stellar evolution from Marigo et al. (2013). Each of these models only differs in the treatment of the efficiency of the third dredge-up process, as described in Section 5.1. The general agreement between these models and the new data is excellent. Within the set of models, the short dashed curve representing a parameterization of $\lambda_{\rm max} = 0.7\lambda_{\rm max}^{\rm K02}$ for the efficiency of the third dredge-up is able to recover the data very well. A refined agreement is obtained with an empirical calibration of the third dredge-up efficiency as a function of the initial stellar mass (red line). Our observations therefore suggest that the third dredge-up does play a role in governing the growth of the core on the TP-AGB, however we will see later in Section 5.2 that it is not the dominant effect.

(A color version of this figure is available in the online journal.)

following each third dredge-up event and the shorter lifetime of the TP-AGB phase.

It follows that, for a given mass-loss prescription, the measurement of the core-mass growth from the white dwarfs is helpful to constrain the third dredge-up as a function of the progenitor's stellar mass, hence of the age. Based on the observed average relationship shown in Figure 3, we have tentatively calibrated the dredge-up parameter $\lambda_{\rm max}$ as a function of the stellar mass, so as to obtain the best match with the data using our reference mass-loss prescription. The corresponding $\lambda_{\rm max}(M_{\rm initial})$ relation is plotted in Figure 2 as a red curve.

A few interesting implications can be drawn. First, at metallicity $Z_{\rm initial} = 0.02$—corresponding to [Fe/H] $\simeq 0.1$ for the adopted solar mixture—the third dredge-up would occur only in stars with $M_{\rm initial} \gtrsim 2\,M_{\odot}$. Second, in the range $2\,M_{\odot} \lesssim M_{\rm initial} \lesssim 3.0\,M_{\odot}$, its maximum efficiency should increase with the stellar mass from zero up to $\lambda_{\rm max} \approx 0.5$ (see Figure 2). Third, the data seem to suggest that at larger masses, $M_{\rm initial} > 3.0\,M_{\odot}$, the third dredge-up should become progressively less efficient, with $\lambda_{\rm max}$ declining toward low values. The decreasing trend of $\lambda_{\rm max}$ is required to recover the rising trend in the growth of the core mass that the Praesepe cluster white dwarfs seem to suggest. We should note that this indication is at variance with the K02 models, that instead predict larger values for $\lambda_{\rm max}$ at increasing stellar mass. Further investigation on both theoretical and observational grounds is deserved before a conclusion on this aspect can be drawn. Clearly, this may have important implications for the chemical yields produced by more massive TP-AGB stars.

In summary, with the present prescription for the third dredge-up, we expect a modest carbon star formation at metallicity $Z_{\rm initial} \simeq 0.02$, mostly confined in stars with masses $2\,M_{\odot} \lesssim M_{\rm initial} \lesssim 3\,M_{\odot}$. The corresponding final surface C/O ratios remain quite low, $1 < {\rm C/O} \lesssim 1.3$ (last column of Table 3), and the fraction of the TP-AGB lifetime spent in the C-star mode reaches a maximum of $\simeq$23% at $M_{\rm initial} \simeq 2.6\,M_{\odot}$. It is interesting to notice that this result is nicely supported by the recent study of Boyer et al. (2013), that has revealed a dramatic scarcity of carbon stars in the inner disk of Andromeda galaxy, characterized by a high metallicity (i.e., [Fe/H] $\simeq +0.1$), comparable to that considered here.

Finally, we plot in Figure 3 the theoretical curve for the core-mass growth, obtained with our calibrated function for $\lambda_{\rm max}$. Our best-fit model shows consistency within $\sim$2% at all masses.

5.2. Characterizing the Significance of Mass Loss

We investigate the influence of stellar winds in controlling the growth of the core mass by running the same set of TP-AGB models for initial metallicity $Z_{\rm initial} = 0.02$, but adopting four additional options for the mass-loss rates, namely: the classical Reimers (1975, also R75) law, and the popular formulas of Vassiliadis & Wood (1993, also VW93), Blöcker (1995, also B95), and van Loon et al. (2005, also vL05).

Though the Reimers law is known to be inadequate to describe the evolution of the mass-loss rates along the TP-AGB (Blöcker 1995; Schröder & Cuntz 2005; Groenewegen et al. 2009; Cranmer & Saar 2011), it is still a classical reference in many studies and its behavior was taken into account, for instance, to infer the metallicity dependence of the TP-AGB fuel in the stellar population synthesis models of Maraston (2005). In that work, the author concluded that the TP-AGB fuel as a function of age, calibrated on Magellanic Cloud (MC) clusters, would correspond to adopting the Reimers law with $\eta_{\rm R} = 2/3$ in TP-AGB calculations (Renzini & Voli 1981). This value represents quite a low efficiency compared to $\eta_{\rm R} = 5$ as derived by Groenewegen & de Jong (1993) to reproduce the observed AGB star luminosity functions in the LMC. It is therefore interesting to check the Reimers assumption with our new TP-AGB models and the new white dwarf data.

The Vassiliadis & Wood (1993) model, calibrated on the empirical relation between mass-loss rates and pulsation periods of variable AGB stars, has become a reference recipe to describe mass loss during the AGB. As a first approach, we adopt the original formulation (Equations (1) and (2) of VW93).

The Blöcker (1995) relation is also a popular prescription in present-day TP-AGB models, and is characterized by quite a steep luminosity dependence. Following the indications of the original paper of Blöcker (1995), we initially assume the Reimers law with an efficiency parameter $\eta_{\rm R} = 0.2$ and, as soon as the pulsation period in the fundamental mode exceeds 100 days, we then switch to the B95 formula keeping the same efficiency parameter, $\eta_{\rm B} = 0.2$.

Finally, we test the relation derived by van Loon et al. (2005) on the basis of spectroscopic and photometric observations of dust-enshrouded red giants in the LMC. Similarly to the other cases, we first adopt the Reimers law with $\eta_{\rm R} = 0.2$, and then we activate the vL05 formula as the pulsation periods becomes longer than 300 days ($\simeq$ to the minimum period of the stars in vL05 calibration sample).

Table 3
PART 1: Best-fitting TP-AGB Model from Marigo et al. (2013)

$M_{\rm initial}$ ($M_\odot$)	$M_{\rm c,1tp}$ ($M_\odot$)	$M_{\rm final}$ ($M_\odot$)	$\rm Fuel_{core}$ ($\rm Fuel_{total}$) ($M_\odot$)	$t_{\rm TP-AGB}$ (Myr)	$E_{\rm core}$ ($E_{\rm total}$) ($10^9\ L_\odot$ yr)	$\rm Fuel^a_{total}$ ($M_\odot$)	$t^{\rm a}_{\rm TP-AGB}$ (Myr)	$E^{\rm a}_{\rm total}$ ($10^9\ L_\odot$ yr)	$\rm C/O_{final}$ photosphere
1.00	0.518	0.541	0.018 (0.018)	0.785	1.77 (1.77)	0.015	0.456	1.44	0.474
1.05	0.521	0.543	0.017 (0.017)	0.679	1.66 (1.66)	0.014	0.424	1.41	0.463
1.10	0.523	0.546	0.018 (0.018)	0.678	1.78 (1.78)	0.016	0.442	1.56	0.452
1.15	0.522	0.555	0.026 (0.026)	0.989	2.54 (2.54)	0.022	0.618	2.17	0.442
1.20	0.524	0.558	0.026 (0.026)	0.911	2.56 (2.56)	0.023	0.606	2.26	0.431
1.25	0.524	0.565	0.032 (0.032)	1.099	3.11 (3.11)	0.028	0.724	2.74	0.423
1.30	0.526	0.566	0.031 (0.031)	0.980	3.03 (3.03)	0.028	0.693	2.77	0.416
1.35	0.528	0.570	0.033 (0.033)	0.978	3.23 (3.23)	0.031	0.716	3.00	0.410
1.40	0.529	0.576	0.037 (0.037)	1.069	3.64 (3.64)	0.035	0.794	3.39	0.403
1.45	0.529	0.582	0.041 (0.041)	1.156	4.04 (4.04)	0.039	0.869	3.78	0.395
1.50	0.524	0.588	0.050 (0.050)	1.471	4.86 (4.86)	0.045	1.058	4.45	0.388
1.55	0.524	0.594	0.054 (0.054)	1.526	5.28 (5.28)	0.050	1.126	4.88	0.380
1.60	0.528	0.598	0.055 (0.055)	1.390	5.35 (5.35)	0.052	1.096	5.08	0.379
1.65	0.521	0.604	0.064 (0.064)	1.734	6.31 (6.31)	0.060	1.304	5.89	0.383
1.70	0.520	0.609	0.069 (0.069)	1.744	6.76 (6.76)	0.065	1.368	6.41	0.383
1.75	0.514	0.615	0.078 (0.078)	2.069	7.64 (7.64)	0.073	1.545	7.12	0.383
1.80	0.513	0.621	0.083 (0.083)	2.081	8.16 (8.16)	0.079	1.621	7.73	0.383
1.85	0.507	0.627	0.092 (0.092)	2.336	8.98 (8.98)	0.086	1.765	8.43	0.384
1.90	0.499	0.632	0.102 (0.102)	2.896	10.01 (10.01)	0.091	1.847	8.87	0.385
1.93	0.493	0.634	0.108 (0.111)	3.314	10.62 (10.87)	0.095	1.944	9.35	0.494
1.95	0.491	0.634	0.110 (0.114)	3.426	10.77 (11.14)	0.097	1.968	9.52	0.541
2.00	0.498	0.638	0.108 (0.115)	3.148	10.55 (11.30)	0.103	2.014	10.05	0.673
...									
...									
2.05	0.499	0.642	0.109 (0.121)	3.125	10.71 (11.84)	0.109	2.089	10.71	0.789
2.10	0.508	0.647	0.106 (0.122)	2.842	10.42 (11.90)	0.113	2.080	11.08	0.884
2.15	0.511	0.653	0.108 (0.129)	2.825	10.62 (12.68)	0.123	2.183	12.00	1.034
2.20	0.515	0.651	0.104 (0.128)	2.712	10.16 (12.57)	0.123	2.162	12.00	1.101
2.25	0.517	0.650	0.101 (0.129)	2.666	9.91 (12.66)	0.124	2.182	12.17	1.155
2.30	0.524	0.654	0.099 (0.129)	2.467	9.70 (12.66)	0.126	2.113	12.32	1.185
2.40	0.534	0.655	0.092 (0.129)	2.298	9.05 (12.60)	0.126	2.048	12.38	1.258
2.60	0.564	0.670	0.080 (0.126)	1.815	7.84 (12.31)	0.125	1.758	12.26	1.321
2.80	0.597	0.697	0.075 (0.124)	1.465	7.32 (12.15)	0.124	1.465	12.15	1.290
3.00	0.637	0.726	0.068 (0.117)	1.125	6.62 (11.43)	0.117	1.125	11.43	1.208
3.20	0.681	0.763	0.062 (0.104)	0.822	6.08 (10.19)	0.104	0.822	10.19	1.075
3.40	0.724	0.787	0.048 (0.074)	0.509	4.67 (7.28)	0.074	0.509	7.28	0.797
3.60	0.751	0.812	0.046 (0.067)	0.405	4.52 (6.58)	0.067	0.405	6.58	0.710
3.80	0.762	0.832	0.053 (0.073)	0.409	5.16 (7.16)	0.073	0.409	7.16	0.711
4.00	0.773	0.853	0.059 (0.078)	0.404	5.80 (7.60)	0.078	0.404	7.60	0.686
4.20	0.786	0.875	0.066 (0.081)	0.388	6.42 (7.90)	0.081	0.388	7.90	0.643
4.40	0.803	0.898	0.069 (0.079)	0.353	6.73 (7.78)	0.079	0.353	7.78	0.573

Note. [a] Quantities integrated for luminosities $\log(L/L_\odot) > 3.4$, i.e., brighter than the RGB tip.

For each mass-loss prescription, we consider two choices of the third dredge-up efficiency, namely: $\xi_\lambda = 1$, that is the standard case $\lambda^{\rm K02}_{\rm max}$ predicted by Karakas et al. (2002), and $\xi_\lambda = 0$, that corresponds to the absence of any dredge-up event. In this way, for each mass-loss law, we can sample the characteristic dispersion in the core mass growth that derives by variations in the third dredge-up efficiency. In particular, the case of $\xi_\lambda = 0$ yields the upper limit of the core mass increment attainable with a given mass-loss prescription. The results are shown in Figure 4. First, we note that the range of the core mass growth enclosed between $\xi_\lambda = 0$ and $\xi_\lambda = 1$ (hatched areas in Figure 4) anti-correlates with the average efficiency of the mass loss, being quite narrow with the B95 and vL05 relations, while becoming much wider with the R75 law.

The final masses obtained with the Vassiliadis & Wood (1993) formalism compare with the data very well, and are strikingly close to those derived with our reference mass-loss prescription, which is based on the Bedijn (1988) formalism. We recall that both relations are empirically calibrated, but the calibration samples of AGB stars and the measured quantities are different, i.e., pulsation periods for VW93; radii, masses and effective temperatures for the Bedijn (1988)-like method. The convergence of the predictions, and the nice agreement with the new observations, at least for the metallicity under consideration, is a promising step toward a more robust AGB calibration.

In this context, the comparison with the observed core mass growth allows one to reject unsuitable mass-loss efficiencies. For instance, the core-mass increment on the TP-AGB obtained with the Blöcker (1995) relation and $\eta_{\rm B} = 0.2$ is always too small, even invoking the most favorable case of no third dredge-up. The same seems to apply, though to a lesser extent, also

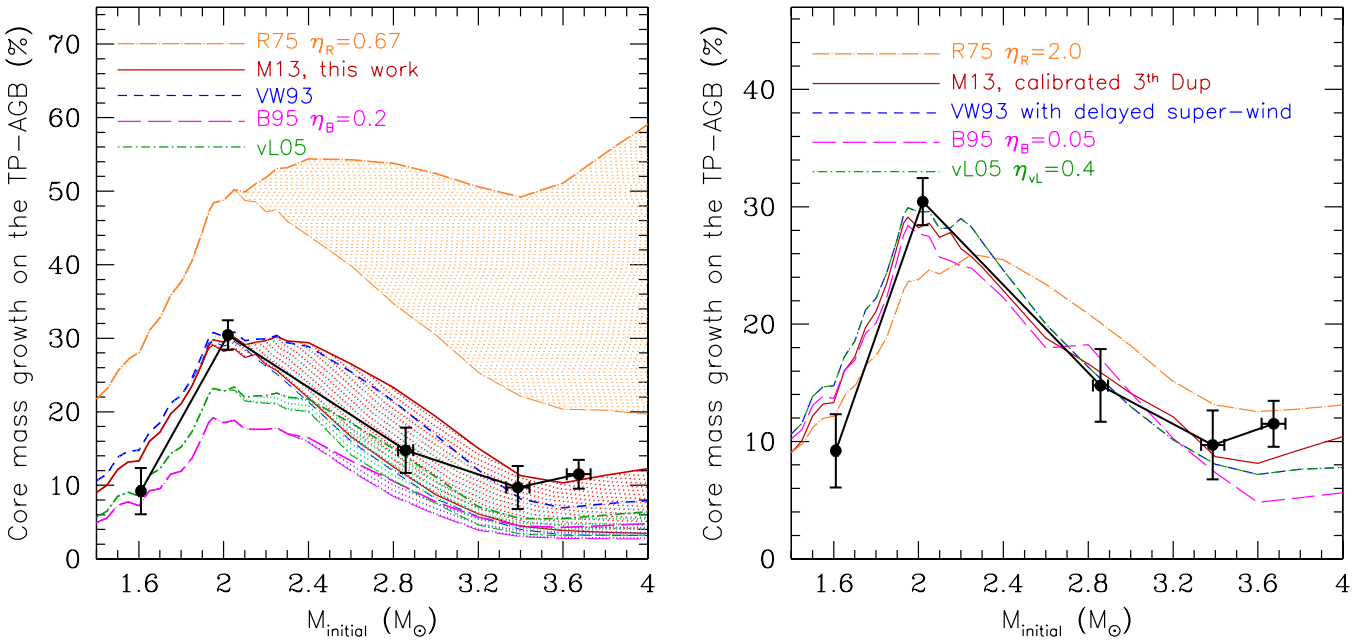

Figure 4. Same as in Figure 3, but showing the predictions with five different descriptions for mass loss on the TP-AGB phase, namely: the Reimers law (R75; orange curves), our reference prescription (Marigo et al. 2013; red curves), the Vassiliadis & Wood (1993, VW93; blue curves), the Blöcker (1995, B95; magenta curves), and the van Loon et al. (2005, vL05; green curves). Left panel: for each mass-loss case, the hatched region encompasses the range of core mass growth expected when varying the third dredge-up efficiency between two extremes, namely: $\xi_\lambda = 1$ (the original K02 prescription; thin line) and $\xi_\lambda = 0$ (no dredge-up; thick line). The latter case corresponds to the maximum growth of the core mass allowed by the corresponding mass-loss relation. Right panel: results obtained with modified versions of the same mass-loss prescriptions (except for the Marigo et al. 2013 case), adopting suitable efficiency parameters or revised relations so as to approach the observational constraints in our study.

(A color version of this figure is available in the online journal.)

to the van Loon et al. (2005) empirical relation. The adopted B95 and vL05 mass-loss formulations do not allow the core to grow enough on the TP-AGB, at least for the case of slightly super-solar initial metallicity, $Z_{\rm initial} \simeq 0.02$ (or equivalently, [Fe/H] $\simeq 0.1$). We note that the high efficiencies of the B95 and L05 mass-loss relations are related to different functional dependences. While the strength of the B95 relation is mostly controlled by the increase in luminosity ($\dot{M}_{\rm B95} \propto L^{4.2}$), hence being particularly efficient in more massive AGB experiencing hot bottom burning (HBB), the intensity of the vL05 mass loss is dictated by the steep sensitivity to the effective temperature ($\dot{M}_{\rm vL05} \propto T_{\rm eff}^{-6.3}$), so that it is expected to affect particularly TP-AGB models of higher metallicities, like those considered in this work.

Contrary to the B95 and vL05 mass-loss rates, the opposite problem arises with the Reimers law adopting $\eta_{\rm R} = 2/3$: the predicted mass loss is too weak, leading to an overestimate of the growth of the core, unless one were to assume that the efficiency of the third dredge-up remains close to unity for most of the TP-AGB evolution at any stellar mass. As a trial, we have considered the case of an extremely strong third dredge-up, taking a high value of the multiplicative factor for the maximum efficiency, $\xi_\lambda = 1.5$, and forcing an earlier onset of the mixing events by setting a lower temperature parameter, $\log(T_{\rm dred}) = 6.3$. We find that the increase of the core mass is now lower, but still too high compared to the observation by roughly 50% at any initial stellar mass. Moreover, such a deep third dredge-up leads to an efficient carbon star formation and quite large surface C/O ratios, of up to 4–5. This prediction seems unrealistic considering that, instead, Galactic carbon stars normally exhibit C/O ratios of just over unity, in any case never exceeding 1.8–2.0 (Lambert et al. 1986; Ohnaka et al. 2000).

Interestingly, some of these findings are in line with the claims of other studies derived from independent arguments. For instance, lower efficiencies for the Blöcker (1995) relation have been adopted by Ventura et al. (2000) ($\eta_{\rm B} = 0.01$) to reproduce the luminosity functions of Li-rich giants in the LMC. More recently, Kamath et al. (2010) have found that the B95 anticipates the AGB termination at too faint luminosities in models aimed at reproducing observations of AGB stars in MC clusters. In a follow-up study Kamath et al. (2012) suggest that the observed luminosity of the AGB tip MC clusters can be correctly recovered assuming that the pulsation period at which the super-wind starts in the VW93 mass-loss prescription is delayed from $P \simeq 500$ days to $P \simeq 700$–800 days. In this framework it is therefore useful to revise all of these mass-loss prescriptions and to find suitable values of their efficiency parameters, or to introduce other modifications that may improve the comparison with the observations.

The right panel of Figure 4 shows the results obtained by running additional sets of TP-AGB models with $Z_{\rm initial} = 0.02$. In all cases we adopt the relation for the third dredge-up efficiency corresponding to $\xi_\lambda = 0.7$, while varying the mass-loss rates. Specifically, we assume the following set of parameters: $\eta_{\rm R} = 2.0$ in the Reimers (1975) law; $\eta_{\rm B} = 0.05$ in the Blöcker (1995) formula; inclusion of the multiplicative factor $\eta_{\rm vL} = 0.4$ in the van Loon et al. (2005) relation; delayed onset of the super-wind in the Vassiliadis & Wood (1993) prescription (their Equation (3)).

Postponing the super-wind in the VW93 mass-loss has the effect of slightly improving the comparison with the data toward

larger stellar masses ($M_{\rm initial}$ >3.0 $M_{\odot}$), allowing a somewhat larger increase of the core mass. For all of the other mass-loss laws, that instead suffered a more significant discrepancy (see left panel of Figure 4), the effect of adjusting the efficiency parameters is substantial, eventually leading to a satisfactory agreement with the observed data in all cases (compare with right panel of Figure 4). We also notice that the majority of the mass-loss relations recover very well the morphology of the observed relation as a function of the initial stellar mass, predicting a peak at $M_{\rm initial} \simeq 2\,M_{\odot}$ and declining wings at both lower and higher masses. The R75 law with $\eta_{\rm R} = 2.0$ produces a somewhat worse trend, as the peak becomes broader and shifted toward larger masses.

As a final remark, we emphasize that the results in Figure 4 show clearly that the main factor controlling the growth of the core mass in TP-AGB stellar models is the adopted mass-loss law. The third dredge-up does play a non-negligible role but, in general, varying its efficiency produces a narrower spread in the final masses than that caused by assuming different mass-loss prescriptions, at least among those proposed in the literature for the TP-AGB phase.

6. THE LIFETIME AND ENERGY OUTPUT OF STARS ON THE TP-AGB

Given their luminous nature and the high level of mass loss suffered, the evolutionary properties of TP-AGB stars are critically important to establish meaningful constraints on the integrated light and chemical yields of stellar populations (e.g., we showed in Section 3 that AGB stars with ∼3 $M_{\odot}$ will lose ∼75% of their mass to the ISM). For decades we have known that, owing to their high intrinsic brightness, TP-AGB stars contribute significantly to the total *bolometric* luminosity of single-burst stellar populations, reaching a maximum of about 40% at ages from 1 to 3 Gyr (Frogel et al. 1990). It is worth noting that these classical estimates are actually quite uncertain and need to be revised, as recently demonstrated by Girardi et al. (2013). The contribution of this phase to the near-IR luminosity may be as high as 80% (see the review of Bruzual 2010, and also see Girardi & Marigo 2007 and Melbourne et al. 2012).

Presently, the treatment of the TP-AGB phase for evolutionary population synthesis models is disputed, leading to large uncertainties in the interpretation of astronomical observations. For example, Maraston et al. (2006) fit the spectral energy distributions of high-redshift *Spitzer* galaxies, and demonstrate that the ages and masses are 60% lower when adopting their TP-AGB models over the Bruzual & Charlot (2003) population synthesis models. On the other side, Kriek et al. (2010) show that the Maraston (2005) models overpredict the rest-frame near-infrared luminosity of a sample of intermediate-redshift post-starburst galaxies. More generally, Conroy (2013) illustrates the strong degeneracy between the modeling of the TP-AGB phase of stellar evolution and the inferred metallicity, stellar mass, and star formation rate of galaxies. The author stresses that the treatment of this phase is essential to avoid large systematic errors in galaxy properties.

A careful reconsideration of the TP-AGB phase, mainly in terms of its evolutionary properties as a function of age and metallicity, is therefore necessary at this stage. Recently, Girardi et al. (2010) introduced a new way of calibrating the TP-AGB phase by directly comparing the number counts of AGB stars predicted on the color–magnitude diagram to that measured in a dozen nearby (low-metallicity) galaxies (from the *Hubble Space Telescope* ANGST/ANGRRR survey—Dalcanton et al. 2009). The results show a dramatic improvement over the older models, both in terms of the TP-AGB tip luminosity and the general luminosity function. The end product of this stellar evolution, with the new mass loss prescription (based on a Bedijn 1988 -like formalism), suggests a white dwarf mass with $M_{\rm final}$ = 0.52–0.54 $M_{\odot}$ for $M_{\rm initial}$ = 0.75–0.85 $M_{\odot}$. This prediction is in exact agreement with the measured remnant mass in the old, metal-poor globular cluster M4, $M_{\rm final} = 0.53 \pm 0.01\,M_{\odot}$ (Kalirai et al. 2009; Kalirai 2012).

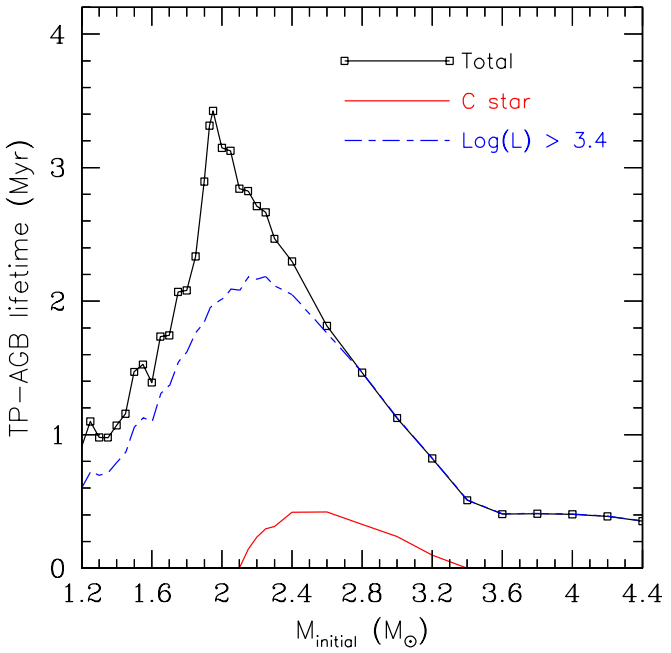

Figure 5. Lifetime of the TP-AGB phase from the Marigo et al. (2013) models with initial metallicity $Z_{\rm initial} = 0.02$, and adopting a calibrated $\lambda_{\rm max}$ relation for the maximum efficiency of the third dredge-up. The time spent at luminosities higher than the RGB tip, i.e., $\log(L/L_{\odot}) \simeq 3.4$, is also shown (blue dashed line), together with the C-star lifetime (red solid line). The predicted TP-AGB core-mass growth in these models fits our new measurements very nicely, as demonstrated in Section 5.1. At the peak core-mass growth in stars with $M_{\rm initial}$ ∼2 $M_{\odot}$, the lifetime of stars in the TP-AGB is τ ∼ 3.4 Myr, which reduces to ∼2 Myr if we consider the TP-AGB portion brighter than the RGB tip. For stars with $M_{\rm initial} \sim 3\,M_{\odot}$, the TP-AGB lifetime is τ ∼ 1 Myr, which drops to $\tau \sim 0.45$ Myr for $M_{\rm initial} \sim 3.5\,M_{\odot}$.

(A color version of this figure is available in the online journal.)

As discussed above, the new TP-AGB evolutionary models in Marigo et al. (2013) present several advances over previous generation models (e.g., Marigo & Girardi 2007), and are found to be in excellent agreement with the independent observations in the present study. In the discussion that follows, we reference core-mass growth and associated yields based on this best-fitting model from Marigo et al. (2013), with calibrated $\lambda_{\rm max}$ relation, shown in Figures 2 and 3. The corresponding evolutionary lifetime of TP-AGB stars with $Z_{\rm initial} = 0.02$ are illustrated in Figure 5. The lifetime of stars on the TP-AGB increases rapidly from $\tau = 1.4$ to 3.4 Myr for stars with $M_{\rm initial} = 1.6$ to ∼1.95 $M_{\odot}$, and then decreases to τ ∼ 2 Myr for $M_{\rm initial} = 2.5\,M_{\odot}$, τ ∼ 1 Myr for $M_{\rm initial} = 3.0\,M_{\odot}$, and $\tau \sim 0.45$ Myr for $M_{\rm initial} = 3.5\,M_{\odot}$.

The peak in the TP-AGB lifetime takes place in correspondence to the stellar progenitor whose mass is the closest to the maximum mass, $M_{\rm HeF}$, for a star to experience the He-flash in the degenerate core at the tip of the red giant branch (RGB). In fact, for $M_{\rm initial} \simeq M_{\rm HeF}$ stellar evolution models expect a minimum in the core mass at the first thermal pulse (e.g., Lattanzio 1986; Bressan et al. 2012). Therefore, stars with

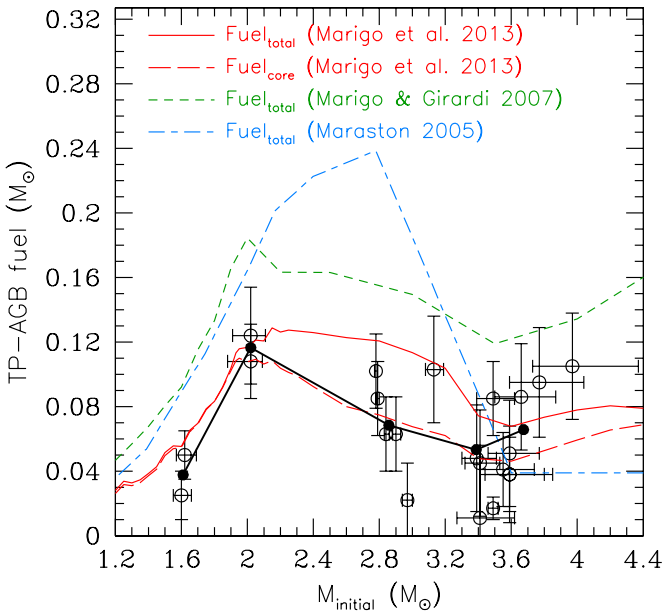

Figure 6. Amount of fuel burnt during the TP-AGB. The red curves are taken from the best-fit (see Section 5.1) model of Marigo et al. (2013), for $Z_{\rm initial} = 0.02$ and the calibrated $\lambda_{\rm max}$ function for the maximum efficiency of the third dredge-up. The long-dashed curve shows the TP-AGB fuel related to the net core-mass growth (i.e., compare to data points in black), whereas the solid curve shows the total TP-AGB fuel (e.g., also including the part of the fuel that escapes the star in the form of chemical yields). For the best-fit model, the fuel burnt through the core-mass growth alone is 90%–65% of the total TP-AGB fuel at $M_{\rm initial} = 2$–$3.5\ M_\odot$. As a comparison, the total fuel burnt on the TP-AGB in the Maraston (2005; long-dashed short-dashed blue curve) and Marigo & Girardi (2007; short-dashed green line) models are also shown. Both predictions are, to different extents, significantly larger than our best-fit model would indicate. This fuel is directly proportional to the energy output during the TP-AGB phase, which we illustrate in Figure 7.

(A color version of this figure is available in the online journal.)

initial masses close to this limit enter the TP-AGB phase at fainter luminosities compared to their neighbors in mass, normally below the tip of the RGB. The net effect is a longer duration of the TP-AGB phase just in proximity of $M_{\rm HeF}$, that is $\simeq 1.95\ M_\odot$ for the chemical composition considered here.

The energy output provided by a star during its TP-AGB phase is simply the time integral of the luminosity over the TP-AGB lifetime, and is proportional to the total amount of nuclear fuel burnt during the evolutionary phase (Renzini & Buzzoni 1986). More recent studies (Marigo & Girardi 2001; Bird & Pinsonneault 2011) have pointed out that the core-mass growth on the TP-AGB provides only a *lower limit* to the total fuel consumption, since part of the nuclear fuel may either be taken away from the core by dredge-up events, or occur outside the core, like in the case of hot-bottom burning in more massive AGB stars. The part of nuclear fuel not locked in the core is eventually lost by the stars in the form of chemical yields, as extensively discussed in Marigo & Girardi (2001).

In Figure 6, we illustrate the fuel burnt on the TP-AGB from the best-fit model, both for the fuel just related to the growth of the stellar core (dashed red curve) and the total fuel (solid red curve). From near the peak fuel consumption at $M_{\rm initial} \sim 2\ M_\odot$ to $3.5\ M_\odot$, the core-mass growth accounts for 90 to 65% of the total TP-AGB fuel. The model predictions for the amount of fuel burnt through the core-mass growth are in excellent agreement with our data points (black points and solid line). For this set of calculations we find that the fraction of the total fuel expelled in the form of chemical yields is zero for $M_{\rm initial} \lesssim 1.9 M_\odot$, then it increases up to $\simeq$40% for $M_{\rm initial} \sim 3\ M_\odot$, and finally decreases to $\simeq$25% for $M_{\rm initial} \sim 4\ M_\odot$.

For comparison, we also illustrate the total TP-AGB fuel predicted by the Marigo & Girardi (2007) and Maraston (2005) models, for $Z_{\rm initial} = 0.019$ and $Z_{\rm initial} = 0.02$, respectively. Both curves are higher than the total fuel expected from our best-fit set of TP-AGB calculations. At initial masses $M_{\rm initial} \sim 1.6, 2.0, 2.8, 3.0\ M_\odot$ the Marigo & Girardi (2007) and Maraston (2005) models exceed our calibrated TP-AGB fuel roughly by 65%, 57%, 26%, 66%, and 61%, 41%, 90%, 16%, respectively.

Following the prescription in Marigo & Girardi (2001), it is straightforward to convert the amount of fuel burnt through the core-mass growth to establish a lower limit of the integrated luminosity emitted during the TP-AGB phase. This result depends only on the measured core-mass growth, the efficiency of H-burning reactions ($A_{\rm H} = 9.79 \times 10^{10}\ L_\odot$ yr, Marigo & Girardi 2001), and the surface abundance of H. The results are illustrated in Figure 7. As above, the red dashed curve is the output energy associated with just the core-mass growth and is in excellent agreement with the data (black points and black solid curve). The solid red curve is the same model, but for the total energy. The TP-AGB energy output is therefore $E \simeq 11$–$12 \times 10^9\ L_\odot$ yr for stars with $2\ M_\odot \lesssim M_{\rm initial} \lesssim 3\ M_\odot$, and then decreases for higher mass stars down to $E = 6$–$7 \times 10^9\ L_\odot$ yr for stars with $3.5\ M_\odot \lesssim M_{\rm initial} \lesssim 4.5\ M_\odot$.

We present theoretical predictions of the TP-AGB core mass at the first thermal pulse, final mass at the end of the TP-AGB, fuel consumed, stellar lifetime, and stellar energy output, final surface C/O ratio, based on the best-fitting model from Marigo et al. (2013) in Table 3. In Table 4, we derive these quantities, other than C/O, for each of the stars in our data set.

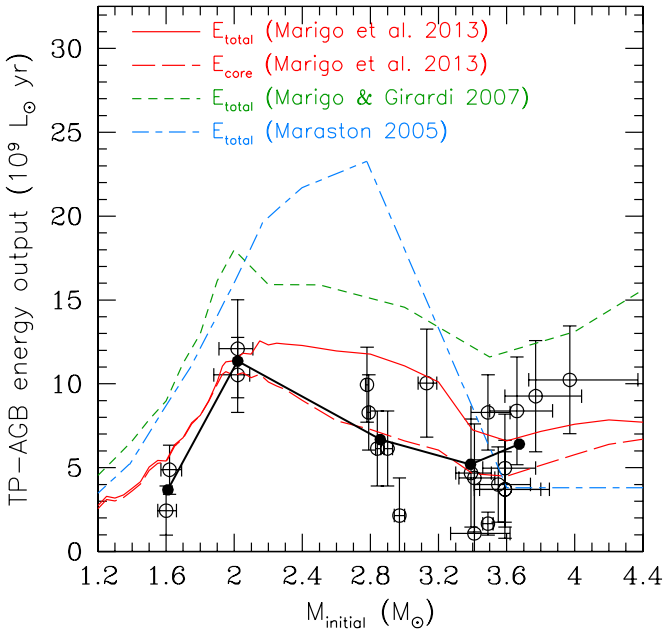

Figure 7. Derived TP-AGB energy output from the best-fit model discussed earlier, both for the energy that results from the net core mass growth (dashed red curve) and the total energy (solid red curve). The black data points and black solid curve illustrate the new observational constraints from our study, which agree nicely with this model. The TP-AGB energy output is $E = 12 \times 10^9\ L_\odot$ yr for stars with $M_{\rm initial} \sim 2\ M_\odot$, and steadily decreases for higher mass stars down to $E = 6.1 \times 10^9\ L_\odot$ yr for stars with $M_{\rm initial} \sim 3.5\ M_\odot$.

(A color version of this figure is available in the online journal.)

Table 4
Measurements of TP-AGB Core-mass Growth, Fuel, and Energy Output

$M_{\rm initial}$ ($M_\odot$)	$M_{\rm final}$ ($M_\odot$)	$M_{\rm c,1tp}$ ($M_\odot$)	$\Delta M_{\rm growth}$ ($M_\odot$)	Fuel$_{\rm core}$ ($M_\odot$)	$E_{\rm core}$ ($10^9\,L_\odot$ yr)
$1.60^{+0.06}_{-0.05}$	0.560	0.528	0.032 ± 0.020	0.025 ± 0.015	2.43 ± 1.52
$1.62^{+0.07}_{-0.05}$	0.590	0.525	0.065 ± 0.020	0.050 ± 0.015	4.93 ± 1.52
$2.02^{+0.07}_{-0.14}$	0.640	0.498	0.142 ± 0.030	0.108 ± 0.023	10.61 ± 2.24
$2.02^{+0.09}_{-0.11}$	0.660	0.498	0.162 ± 0.040	0.124 ± 0.030	12.11 ± 2.99
$2.78^{+0.01}_{-0.01}$	0.730	0.594	0.136 ± 0.030	0.102 ± 0.023	10.04 ± 2.21
$2.79^{+0.01}_{-0.01}$	0.710	0.597	0.113 ± 0.030	0.085 ± 0.023	8.34 ± 2.21
$2.84^{+0.02}_{-0.01}$	0.690	0.606	0.084 ± 0.030	0.063 ± 0.023	6.20 ± 2.21
$2.90^{+0.03}_{-0.02}$	0.700	0.617	0.083 ± 0.030	0.063 ± 0.023	6.13 ± 2.21
$2.97^{+0.03}_{-0.03}$	0.660	0.631	0.029 ± 0.030	0.022 ± 0.023	2.14 ± 2.22
$3.13^{+0.06}_{-0.05}$	0.802	0.665	0.137 ± 0.043	0.103 ± 0.033	10.13 ± 3.18
$3.39^{+0.12}_{-0.09}$	0.785	0.721	0.064 ± 0.043	0.048 ± 0.033	4.74 ± 3.19
$3.41^{+0.12}_{-0.09}$	0.785	0.726	0.059 ± 0.043	0.045 ± 0.033	4.37 ± 3.19
$3.41^{+0.21}_{-0.14}$	0.740	0.726	0.014 ± 0.060	0.011 ± 0.045	1.04 ± 4.44
$3.49^{+0.13}_{-0.10}$	0.850	0.737	0.113 ± 0.030	0.085 ± 0.023	8.35 ± 2.22
$3.49^{+0.03}_{-0.03}$	0.760	0.737	0.023 ± 0.010	0.017 ± 0.007	1.70 ± 0.74
$3.55^{+0.19}_{-0.14}$	0.800	0.745	0.055 ± 0.030	0.041 ± 0.023	4.06 ± 2.21
$3.59^{+0.18}_{-0.13}$	0.817	0.749	0.068 ± 0.044	0.051 ± 0.033	5.01 ± 3.24
$3.59^{+0.26}_{-0.18}$	0.800	0.749	0.051 ± 0.040	0.038 ± 0.030	3.76 ± 2.95
$3.59^{+0.21}_{-0.15}$	0.800	0.749	0.051 ± 0.030	0.038 ± 0.023	3.76 ± 2.21
$3.66^{+0.21}_{-0.16}$	0.869	0.754	0.115 ± 0.044	0.086 ± 0.033	8.44 ± 3.23
$3.77^{+0.27}_{-0.18}$	0.888	0.760	0.128 ± 0.045	0.095 ± 0.034	9.33 ± 3.28
$3.97^{+0.40}_{-0.24}$	0.914	0.771	0.143 ± 0.045	0.105 ± 0.033	10.30 ± 3.24

7. CONCLUSION

The physical processes occurring on the TP-AGB phase of stellar evolution lead to dynamic changes in the nature of stars. Over the course of just a few million years, stars can shed >75% of their mass through winds during this evolution. The theoretical parameterization of these processes plays a critical role in the interpretation of light from unresolved galaxies (especially at intermediate ages), however, such efforts are relatively unconstrained by observations. In this paper, we leverage new discoveries of white dwarfs in the nearby and well-studied Hyades and Praesepe star clusters to establish 18 initial and final mass pairs, combined with earlier studies by our team of the older star clusters NGC 6819 and NGC 7789. These data provide new insights on the properties of the TP-AGB phase of stellar evolution.

We measure the growth of the core mass on the TP-AGB to be 10% at $M_{\rm initial} = 1.6$, rising rapidly to 30% at $M_{\rm initial} \simeq 2.0\,M_\odot$. For more massive stars, the core-mass growth is lower and decreases steadily to ∼10% at $M_{\rm initial} \simeq 3.4\,M_\odot$. These results are in nice agreement with the new TP-AGB models in Marigo et al. (2013) for initial metallicity $Z_{\rm initial} = 0.02$, which offer several advances over previous generation calculations. By comparing to models with varying efficiencies of the third dredge-up and different mass-loss prescriptions, we demonstrate that the stellar mass loss rate plays the dominant role in guiding the core-mass growth, but the third dredge-up also produces an important effect that must be taken into account.

We find that the semi-empirical Bedijn (1988)-like relation (adopted in Marigo et al. 2013) and the Vassiliadis & Wood (1993) formula yield a very good agreement with the new white dwarfs mass measurements, while other prescriptions in the literature need to be tuned by adjusting ad-hoc multiplicative factors. Our exploratory calibration (see Figure 2) suggests to adopt $\eta_{\rm B} \simeq 0.05$ in the Blöcker (1995) formula, $\eta_{\rm vL} \simeq 0.4$ in the van Loon et al. (2005) relation, and $\eta_{\rm R} \simeq 2$ in the Reimers (1975) law. We note, however, that this latter law produces less satisfactory results, failing to reproduce the morphology of the observed relation between the core-mass growth and the initial stellar mass, and in general, it should not be considered a suitable choice for the TP-AGB phase.

A tentative calibration of the third dredge-up efficiency at metallicities $Z_{\rm initial} = 0.02$, as a function of the stellar mass would indicate that i) stars with $M_{\rm initial} < 1.9\ M_\odot$ do not experience the third dredge-up, in agreement with predictions of full AGB models (Karakas et al. 2002); ii) at larger masses the efficiency of the third dredge-up increases quickly with the stellar mass up to values $\lambda_{\rm max} \simeq 0.5$ for $M_{\rm initial} \simeq 2.5$–$3.0\,M_\odot$; iii) this positive trend is eventually reversed and the third dredge-up becomes less efficient with increasing stellar mass, illustrating a larger core-mass growth. The latter point is at odds with full TP-AGB models (Karakas et al. 2002) that predict $\lambda_{\rm max} \simeq 0.9$–$1.0$ for $M_{\rm initial} < 4.0\ M_\odot$. Given its critical impact on the chemical yields from more massive AGB stars, this aspect demands a further careful analysis, which is postponed to a follow-up work. In any case, the inefficient C-star formation at $Z_{\rm initial} = 0.02$, that follows from this preliminary calibration, is supported by the recent study of Boyer et al. (2013), who have pointed out a dramatic scarcity of C stars in the inner disk of the M31 galaxy, a region characterized by a metallicity comparable to that considered in this work ([Fe/H] ≃ +0.1).

Finally, we relate the core-mass growth to the nuclear fuel burnt during the TP-AGB phase to calculate the energy output of stars in this phase as summarized in Tables 3 (best-fitting model) and 4 (data). At the peak core-mass growth for stars with $M_{\rm initial} \sim 2\,M_\odot$, the TP-AGB lifetime is $\tau \simeq 3.4$ Myr, which reduces to $\tau \simeq 2$ Myr for luminosities brighter than the RGB tip (i.e., $\log(L/L_\odot) > 3.4$). The corresponding integrated luminosity is $L \simeq 12 \times 10^9\,L_\odot$ yr.

Our measurements illustrate that the fuel burnt during the TP-AGB for metallicity $Z_{\rm i} \simeq 0.02$, is substantially lower than adopted by Maraston (2005), and to a lesser extent, than predicted by Marigo & Girardi (2007). This finding is in line with other recent studies that, from independent arguments, favor a *lighter* TP-AGB contribution to the integrated galaxy light, (e.g., Kriek et al. 2010; Melbourne et al. 2012; Zibetti et al. 2013; Conroy 2013). Our results are also in line with the recent conclusions of Girardi et al. (2013), who point out at an insidious problem in present derivations of the TP-AGB fuel based on MC star clusters.

We caution that the conclusions drawn from this study apply to the TP-AGB stars with slightly super-solar metallicity, and a straightforward extrapolation to lower metallicities is not correct and should be avoided. Accomplishing a thorough and reliable TP-AGB calibration requires an observational sampling over the entire relevant ranges of ages and metallicites. Accurate white dwarf mass measurements in additional intermediate-aged star clusters, like those presented in this work, provide us with a valuable contribution to achieve this ambitious and challenging goal.

We wish to thank L. Girardi for providing us with the latest stellar evolution models to translate stellar lifetimes into masses. We also wish to thank Jonathan Bird and Marc Pinsonneault for several useful discussions, and Brad Hansen for leading the Keck spectroscopic proposal that led to the

white dwarf measurements in NGC 6819 and NGC 7789. We acknowledge the help of the team in the Kalirai et al. (2008) study for the initial measurements. This project was supported by the National Science Foundation (NSF) through grant AST-1211719. P.M. acknowledges financial support from *Progetto di Ateneo 2012*, ID-CPDA125588/12, University of Padova. P-E.T. was supported during this project by the Alexander von Humboldt Foundation and by NASA through Hubble Fellowship grant HF-51329.01, awarded by the Space Telescope Science Institute, which is operated by the Association of Universities for Research in Astronomy, Incorporated, under NASA contract NAS5-26555.

REFERENCES

An, D., Johnson, J. A., Clem, J. L., et al. 2008, ApJS, 179, 326
Anthony-Twarog, B. J. 1982, ApJ, 255, 245
Anthony-Twarog, B. J. 1984, AJ, 89, 267
Bedijn, P. J. 1988, A&A, 205, 105
Bergeron, P., Saffer, R. A., & Liebert, J. 1992, ApJ, 394, 228
Bird, J. C., & Pinsonneault, M. H. 2011, ApJ, 733, 81
Blöcker, T. 1995, A&A, 297, 727
Boyer, M. L., Girardi, L., Marigo, P., et al. 2013, ApJ, 774, 83
Bressan, A., Marigo, P., Girardi, L., et al. 2012, MNRAS, 427, 127
Bruzual, A. G. 2010, in IAU Symp. 262, Stellar Populations—Planning for the Next Decade, ed. G. R. Bruzual & S. Charlot (Cambridge: Cambridge Univ. Press), 55
Bruzual, G. A., & Charlot, S. 2003, MNRAS, 344, 1000
Caffau, E., Ludwig, H.-G., Steffen, M., Freytag, B., & Bonifacio, P. 2011, SoPh, 268, 255
Casewell, S. L., Dobbie, P. D., & Napiwotzki, R. 2009, MNRAS, 395, 1795
Claver, C. F., Liebert, J., Bergeron, P., & Koester, D. 2001, ApJ, 563, 987
Conroy, C. 2013, ARA&A, 51, 393
Conroy, C., & Gunn, J. E. 2010, ApJ, 712, 833
Conroy, C., Gunn, J. E., & White, M. 2009, ApJ, 699, 486
Cranmer, S. R., & Saar, S. H. 2011, ApJ, 741, 54
Dalcanton, J., Williams, B. F., Seth, A. C., et al. 2009, ApJS, 183, 67
Dobbie, P. D., Napiwotzki, R., Burleigh, M. R., et al. 2006, MNRAS, 369, 383
Dobbie, P. D., Pinfield, D. J., Napiwotzki, R., et al. 2004, MNRAS, 355, L39
Eggen, O. J., & Greenstein, J. L. 1965, ApJ, 141, 83
Frogel, J. A., Mould, J., & Blanco, V. M. 1990, ApJ, 352, 96
Girardi, L., & Marigo, P. 2007, A&A, 462, 237
Girardi, L., Marigo, P., Bressan, A., & Rosenfield, P. 2013, ApJ, 777, 142
Girardi, L., Williams, B. F., Gilbert, K. M., et al. 2010, ApJ, 724, 1030
Gratton, R. 2000, in ASP Conf. Ser. 198, Stellar Clusters and Associations: Convection, Rotation, and Dynamos, ed. R. Pallavicini, G. Micela, & S. Sciortino (San Francisco: CA: ASP), 225
Groenewegen, M. A. T., & de Jong, T. 1993, A&A, 267, 410
Groenewegen, M. A. T., Sloan, G. C., Soszyński, I., & Petersen, E. A. 2009, A&A, 506, 1277
Gustafsson, B., & Höfner, S. 2004, in Asymptotic Giant Branch stars, ed. H. J. Habing & H. Olofsson (New York: Springer), 149
Habing, H. J. 1996, ARA&A, 7, 97
Herwig, F. 2004, ApJ, 605, 425
Herwig, F. 2005, ARA&A, 43, 435
Kalirai, J. S. 2012, Natur, 486, 90
Kalirai, J. S., Bergeron, P., Hansen, B. M. S., et al. 2007, ApJ, 671, 748
Kalirai, J. S., Davis, S. D., Richer, H. B., et al. 2009, ApJ, 705, 408
Kalirai, J. S., Hansen, B. M. S., Kelson, D. D., et al. 2008, ApJ, 676, 594
Kalirai, J. S., Richer, H. B., Fahlman, G., et al. 2001, AJ, 122, 266
Kalirai, J. S., Richer, H. B., Reitzel, D., et al. 2005, ApJL, 618, L123
Kamath, D., Karakas, A. I., & Wood, P. R. 2012, ApJ, 746, 20
Kamath, D., Wood, P. R., Soszyński, I., & Lebzelter, T. 2010, MNRAS, 408, 522
Karakas, A. I., Lattanzio, J. C., & Pols, O. 2002, PASA, 19, 515
Kleinman, S. J., Kepler, S. O., Koester, D., et al. 2013, ApJS, 204, 5
Kriek, M., Labbé, I., Conroy, C., et al. 2010, ApJL, 722, L64
Lambert, D. L., Gustafsson, B., Eriksson, K., & Hinkle, K. H. 1986, ApJS, 62, 373
Lattanzio, J. C. 1986, ApJ, 311, 708
Luyten, W. J. 1962, The Observatory, Univ. Minnesota, 31, 1
Maraston, C. 2005, MNRAS, 362, 799
Maraston, C., Daddi, E., Renzini, A., et al. 2006, ApJ, 652, 85
Marigo, P. 2002, A&A, 387, 507
Marigo, P. 2012, in IAU Symp. 283, Planetary Nebulae: An Eye to the Future, ed. A. Manchado, L. Stanghellini, & D. Schönberner (Cambridge: Cambridge Univ. Press), 87
Marigo, P. 2013, in IAU Symp. 281, Binary Paths to Type Ia Supernovae Explosions, ed. R. DiStefano, M. Orio, & M. Moe (Cambridge: Cambridge Univ. Press), 36
Marigo, P., & Aringer, B. 2009, A&A, 508, 1539
Marigo, P., Bressan, A., Nanni, A., Girardi, L., & Pumo, M. L. 2013, MNRAS, 434, 488
Marigo, P., & Girardi, L. 2001, A&A, 377, 132
Marigo, P., & Girardi, L. 2007, A&A, 469, 239
Marigo, P., Girardi, L., & Bressan, A. 1999, A&A, 344, 123
Marigo, P., Girardi, L., Bressan, A., et al. 2008, A&A, 482, 883
Mattsson, L., Wahlin, R., & Höfner, S. 2010, A&A, 509, A14
Melbourne, J., Williams, B. F., Dalcanton, J. J., et al. 2012, ApJ, 748, 47
Miglio, A., Brogaard, K., Stello, D., et al. 2012, MNRAS, 419, 2077
Ohnaka, K., Tsuji, T., & Aoki, W. 2000, A&A, 353, 528
Perryman, M. A. C., Brown, A. G. A., Lebreton, Y., et al. 1998, A&A, 331, 81
Reid, N. 1992, MNRAS, 257, 257
Reimers, D. 1975, MSRSL, 8, 369
Renzini, A., & Buzzoni, A. 1986, in Spectral Evolution of Galaxies, ed. C. Chiosi & A. Renzini (Astrophysics and Space Science Library, Vol. 122; Dordrecht: Reidel), 195
Renzini, A., & Voli, M. 1981, A&A, 94, 175
Schilbach, E., & Röser, S. 2012, A&A, 537, A129
Schröder, K.-P., & Cuntz, M. 2005, ApJL, 630, L73
Tremblay, P.-E., & Bergeron, P. 2009, ApJ, 696, 1755
Tremblay, P.-E., Schilbach, E., Roser, S., et al. 2012, A&A, 547, 99
van Altena, W. F. 1969, AJ, 74, 2
van Loon, J. T., Cioni, M.-R. L., Zijlstra, A. A., & Loup, C. 2005, A&A, 438, 273
Vassiliadis, E., & Wood, P. R. 1993, ApJ, 413, 641
Ventura, P., D'Antona, F., & Mazzitelli, I. 2000, A&A, 363, 605
von Hippel, T. 1998, AJ, 115, 1536
Wagenhuber, J., & Groenewegen, M. A. T. 1998, A&A, 340, 183
Weidemann, V. 2000, A&A, 363, 647
Weidemann, V., Jordan, S., Iben, I. Jr, & S., Casertano 1992, AJ, 104, 1876
Willson, L. A. 2000, ARA&A, 38, 573
Zibetti, S., Gallazzi, A., Charlot, S., Pierini, D., & Pasquali, A. 2013, MNRAS, 428, 1479
Zuckerman, B., Klein, B., Xu, S., & Jura, M. 2013, ApJ, 770, 140